HHS Public Access

Author manuscript

Nat Struct Mol Biol. Author manuscript; available in PMC 2011 January 01.

Published in final edited form as:

Nat Struct Mol Biol. 2010 July ; 17(7): 830–836. doi:10.1038/nsmb.1823.

Structural Changes in a Marine Podovirus Associated with Release of its Genome into *Prochlorococcus*

Xiangan Liu[1], **Qinfen Zhang**[1,2], **Kazuyoshi Murata**[1], **Matthew L. Baker**[1], **Matthew B. Sullivan**[3,4], **Caroline Fu**[1], **Matthew Dougherty**[1], **Michael F. Schmid**[1], **Marcia S. Osburne**[3], **Sallie W. Chisholm**[3], and **Wah Chiu**[1]

[1]National Center for Macromolecular Imaging, Verna and Marrs McLean Department of Biochemistry & Molecular Biology, Baylor College of Medicine, Houston, TX, 77030, USA

[2]State Key lab for Biocontrol, School of Life Sciences, Sun Yat-Sen University, Guangzhou 510275, China

[3]Department of Civil and Environmental Engineering, M.I.T., Cambridge, MA 02139, USA

Abstract

Podovirus P-SSP7 infects *Prochlorococcus marinus*, the most abundant oceanic photosynthetic microorganism. Single particle cryo-electron microscopy (cryo-EM) yields icosahedral and asymmetrical structures of infectious P-SSP7 with 4.6 Å and 9 Å resolution, respectively. The asymmetric reconstruction reveals how symmetry mismatches are accommodated among 5 of the gene products at the portal vertex. Reconstructions of infectious and empty particles show a conformational change of the "valve" density in the nozzle, an orientation difference in the tail fibers, a disordering of the C-terminus of the portal protein, and disappearance of the core proteins. In addition, cryo-electron tomography (cryo-ET) of P-SSP7 infecting *Prochlorococcus* demonstrated the same tail fiber conformation as in empty particles. Our observations suggest a mechanism whereby, upon binding to the host cell, the tail fibers induce a cascade of structural alterations of the portal vertex complex that triggers DNA release.

Cyanophage P-SSP7, categorized as a T7-like podovirus based on morphology and genome sequence[1], is found in *Prochlorococcus*, a genus of marine cyanobacteria from the Atlantic Ocean. The *Prochlorococcus* group, consisting of genetically distinct ecotypes[2], contributes a significant fraction of global oceanic photosynthesis[3], and T7-like phages such as P-SSP7 are among the most abundant viral types observed in viral metagenomes from the vast, low-

[4]Present address: Department of Ecology and Evolutionary Biology, University of Arizona, Tucson, AZ 85721, USA

Accession codes: The density maps and associated models have been deposited to EBI (accession numbers xx to be included in the galley proof).

Note: Supplementary information is available on the Nature Structural & Molecular Biology website.

Author Contributions: M.B.S., M.S.O. and S.W.C provided samples. Q.Z. took single particle images. Q.Z., C.F. and K.M. took tomographic images. X.L. introduced the methodology for single particle symmetric and asymmetric reconstructions; computed all the maps. X.L. and W.C. interpreted the maps. M.F.S. analyzed the difference maps. K.M. did tomographic reconstructions and performed its analysis with M.F.S. assistance. M.L.B. and X.L. built Cα backbone models. M.T.D. and W.C. designed the animations. X.L. and W.C. wrote the paper with contributions from all co-authors.

nutrient (oligotrophic) surface ocean waters[4]. P-SSP7 is one of the best characterized marine phages, as its complete genome has been sequenced[1] and the transcriptomes and proteomes of both the virus and host cell during infection have been described[5,6]. Here, we expand upon these efforts by elucidating the structural features of the viral particle on its own using single particle cryo-EM and during the host infection process using cryo-ET, revealing biologically important phenomena in this system.

Results

Icosahedral reconstruction of P-SSP7 capsid

Using 36,000 particle images (Fig. 1a), we obtained an icosahedral reconstruction of the P-SSP7 shell at ~4.6 Å resolution (Supplementary Fig. 1a,b and Movie 1a) using MPSA[7] and EMAN[8]. The density map shows the phage particle has a *T*=7 shell that is 25–40 Å thick and ~655 Å in diameter from 5-fold to opposite 5-fold vertices. Using a *de novo* model building technique[9], we were able to build the alpha-carbon (Cα) backbone chain trace models for each of the 7 shell proteins (gp10) in an asymmetric unit. Figure 1b shows one of the gp10 models (residues 1–363) containing 5 structural features, 4 of which also appear in other phage capsid structures[9,10] (Supplementary Fig. 2 and Movie 1b): an extended amino terminus (N arm), a triangular domain (Domain A), an elongated protrusion domain (Domain P), a long extended loop (E loop), and a structurally important small loop between the N arm and E loop, near the local 2-fold axis (which we call the F loop).

The backbones of all 7 subunits have slightly different conformations (Supplementary Fig. 1c), but have similar structural features and topology. The whole capsid backbone model is shown in Supplementary Fig. 1d and Movie 1c. The Cα backbone trace of gp10 shows its fold to be topologically similar to the corresponding shell protein of other tailed phages such as ε15[9], HK97[10] (Supplementary Fig. 2), P22[11], T4[12], φ29[13] and of herpes simplex type 1 virus[14], even though no sequence homology is evident. These phages appear to have different ways (Supplementary Fig. 2) of protecting their shells against the high internal pressure (30–60 atm) produced by tight genome packing[15]. P-SSP7 does not have decoration proteins such as those used by ε15 to stabilize its shell, nor does it have a covalently cross-linked chain mail like HK97 (Supplementary Fig. 2). Instead, P-SSP7 uses subunit interactions within and between its capsomeres to stabilize its capsid shell (Fig. 1c,d) in a way that has not been seen previously in other phage structures.

A strong density between capsomeres is found at the F loop between the charged residues, Lys61 of one subunit and Glu120 in the domain P of another subunit (Fig. 1d). The F loop in P-SSP7 is longer than in either HK97 or ε15 and also interacts with the portal to accommodate symmetry mismatch at the portal vertex, as will be seen in the asymmetric reconstruction. Another previously unseen interaction occurs within each capsomere: the N arm (cyan-colored loops in Fig. 1c) of one subunit wraps around the long E loop (Fig. 1c) of a neighboring subunit, thus reducing the flexibility of the E loop without requiring β sheet formation as in HK97. All these capsid shell features of P-SSP7 may be crucial in compensating for lack of cross-linking[10] or an additional protein[9] against the high internal pressure.

Asymmetric reconstruction of the P-SSP7 virion

Due to the symmetry enforcement in the reconstruction above, the density of the portal vertex complex (defined herein as all the densities associated with the special 5-fold vertex) is lost. Traditionally, structures of the non-icosahedral protein components were studied individually by crystallography or NMR and fit to the low-resolution cryo-EM maps of the virion or complexes isolated from virions[16-18]. It has also been possible to identify these components by computationally isolating the tail from single particle images (e.g. T4[19] and SPP1[20]). This divide- and-conquer approach has undeniably contributed much insight into virus structure, assembly and infection. In view of the advances in the cryo-EM method, we opted to determine the structure of the entire mature P-SSP7 phage without any imposed symmetry, to find the detailed structures of the portal vertex complex and the spatial relationships among protein components of the portal vertex complex and the icosahedral shell.

Using the same data set and a newly developed reconstruction algorithm (Supplementary Methods), we produced a ~9 Å resolution density map without assuming any symmetry (Fig. 2, Supplementary Fig. 3a). In comparing the asymmetric density map with the Cα model from the 4.6 Å icosahedrally imposed map, we found that the portal vertex and its opposite 5-fold vertex are compressed along the radius by ~3–4 Å, whereas the other 10 "normal" 5-fold vertices appear to match with those determined from the icosahedral reconstruction. Although the extent of such compression is smaller than the resolution of either map, small differences between structures can be reliably revealed as shown in many structural examples[21,22].

We segmented the densities at the portal vertex of the map into the following components: nozzle, adaptor, tail fibers, portal and core proteins (Fig. 2a,b). This segmentation assignment is based on the following considerations: (1) the connectivity of the densities, (2) the classification of different protein parts of T7 phage[23], (3) the match of the detected secondary structure elements in both the adaptor and nozzle to the sequence based predictions of gp11 and gp12 (Supplementary Figs 4 and 5), and (4) the match of both the capsid model (Fig. 1b) and homologs of the portal (Supplementary Fig. 6) to their corresponding densities.

The cryo-EM map, along with genomics[1] and proteomics[5] studies of P-SSP7 and previous T7 biochemical studies[23], allowed us to annotate the segmented densities at the portal vertex complex in terms of the corresponding gene products (Supplementary Methods). These include the adaptor (gp11), nozzle (gp12), tail fiber (gp17), portal (gp8), and the dsDNA genome (Fig. 2b and Supplementary Movie 2). Each of these densities (adaptor, nozzle, portal) is also cross-validated by the expected volumes of the putative gene products. However, the nozzle may contain slightly more volume than six copies of gp12 would occupy.

The 9 Å resolution map of P-SSP7 is sufficient to determine the copy number and symmetry for most of the protein components in the portal vertex complex using rotational correlation analysis. The analyses (Supplementary Fig. 3d) show 12 copies for the portal protein and 6 copies for the nozzle protein with 12 and 6 fold symmetries respectively. The 12 adaptor

proteins have weak 6-fold symmetry near the nozzle and 12-fold symmetry at the opposite end near the portal (Supplementary Fig. 3d). The 12 copies of the adaptor protein exist in two conformations that have alternating positions in the ring-shaped adaptor (Fig. 3c). Each of the 6 tail fibers appears to be a trimer (Fig. 2c), which splays out into three “petals” and then rejoins at the junction with the adaptor and nozzle (Fig. 2c,d). Since the visible length and size of each tail fiber can account for only part of its trimer, the distal portion must be very flexible and therefore not visible in our asymmetric reconstruction. The inner core proteins are poorly defined, and no symmetry could be identified.

Applying the appropriate symmetry to some of the portal vertex protein components, the contrast of their structural features can be enhanced. Using SSEHunter[24] to analyze of the symmetrized components, we were able to identify α-helices (>2 turns) and β-sheets (> 2 strands) in these densities: 2 α-helices and 2 β-sheets in the adaptor protein, 8 β sheets in the nozzle protein, 3 β sheets in the tail fiber trimer, and 12 α-helices and 3 β sheets in the portal protein (Supplementary Fig. 4). The accuracy in the identification of these secondary structure elements was substantiated by the positional match of the helices and sheets of the capsid protein (gp10) in this 9 Å map with its structure in the 4.6 Å icosahedral map (Fig. 1b). In addition, we found that our assignment of the identified secondary structure elements agree well with those predicted by bioinformatics tools for both the nozzle protein (gp12, primarily β sheet) and the adaptor protein (gp11, a mixture of α helices and β sheets) (Supplementary Fig. 5).

Despite the absence of a crystal structure of the P-SSP7 portal subunit (gp8, 522 residues), we matched the density and secondary structure elements of the putative portal (gp8) with models of its structural homologs from φ29[25] (1IJG, 309 residues) and SPP1[26] (2JES, 503 residues). We found the upper part of the density has a large conformational difference from the SPP1 portal[26] structure, but the lower part density fits well with both φ29 and SPP1 portal structures (Supplementary Fig. 6a,b). This match further supports the accuracy of our secondary structure element identification and segmentation of gp8. Based on the sequence alignment between the φ29 portal and the P-SSP7 portal protein, we can deduce that the unmatched density, which points towards the center of the capsid, belongs to the C-terminus (Supplementary Fig. 6a,b). Furthermore, the consensus secondary structure prediction (Supplementary Fig. 6c) of the gp8 C-terminal region (residues 473–497) suggests that it is an α-helix with a glutamine (Q)-rich motif, in agreement with our SSEHunter results (Supplementary Fig. 6d). This has not been seen previously in other phage portal protein structures but, interestingly, sequence analysis[27],[28] also predicts α-helices near the C-termini of portal proteins in other phages (T7, syn5, KIE, ε15). In P-SSP7, a total of 12 Q-rich helix cluster motifs near the C terminus of the portal are surrounded by the inner core proteins. Q-rich motifs are known to undergo reversible assembly and disassembly in protein complexes[29]; the Q-rich domain here may play some role in the disassembly and assembly of the internal core proteins, DNA translocation, and/or stabilization of the DNA terminus. Such functional speculation requires future experimental verification.

In the asymmetric reconstruction, the putative core protein density is the most difficult region to interpret (Fig. 2b). As suggested previously, gp15 and gp16 and possibly gp14 are core components[1],[5]. Because we cannot assign a copy number, observe any symmetry or

resolve any discernable secondary structure elements in the observed core density, we cannot tell if this density is made of any or all of these three gene products. In addition, the genomics and proteomics analyses have proposed several other gene products with completely unknown functions and localizations (i.e. orf 23, 37, 38, 39, 41, 42, 46, 48, 50)[1,5]. These unknown proteins may have a small number of copies, be very flexible or be attached to other flexible components. The resolution of our map is still too limited to determine whether these proteins correspond to any of the observed densities.

The size of the capsid chamber can accommodate the 44,970 base pairs (bp) genome[1] which is packed coaxially around the portal vertex axis with a spacing of ∼24 Å between rings (Fig. 2b, Supplementary Fig. 3c). The rings are packed hexagonally (Fig. 2b). The DNA near the inner capsid surface is better resolved than the rest of the DNA, suggesting possible interactions between the capsid and the DNA. We tentatively interpret the relatively strong density filling the channel in the portal vertex (250 Å long, ∼73bp and ∼20 Å wide) to be the DNA terminus. Density at this location was also observed in ε15 phage[30]. This density extends as far as the interface between the nozzle and the adaptor. A density protruding from the 6 nozzle proteins towards the central axis appears to cap the tip of the DNA terminus, which we annotate as the “nozzle valve” (Figs 2b–d and 3e).

There is a split of the density resulting in a separation of ∼14 Å in the middle of the DNA terminus (Fig. 2b, Supplementary Fig. 3c), which we interpret as strand separation caused by the torsional strain on the double-stranded DNA during packaging[31], and/or specific interactions of the flipped-out bases with the portal. Each individual strand density is ∼8 Å in diameter. Thus, the size of the separated strands in our map is consistent with single-stranded DNA rather than with double-stranded DNA. The separation occurs near the center of the portal, whereas the proposed toroidal dsDNA structure of φ29 phage[32] occurs on the outside end of its portal. The size of the 14 Å separation seems too small to accommodate a loop or torus of double stranded DNA as found in phage φ29. Therefore, these DNA features are completely different between P-SSP7 and φ29.

Symmetry mismatch at the portal vertex

Symmetry mismatch between the 5-fold capsid and the portal vertex complex has been observed in dsDNA phages[26,30,33,34]. Our asymmetric map (Fig. 2a) shows how the portal (gp8) and capsid proteins (gp10) accommodate the 5-fold and 12-fold mismatch at the molecular level. Where the portal complex occurs instead of a penton at the portal vertex in our map, there are 10 gp10 proteins that surround the 12 gp8 portal proteins. The interfacial density (Fig. 3a) reveals four interaction types (Fig. 3b): five portal subunits (2,4,7,9,12) contact the F loop of cyan-colored gp10 subunits, another 5 portal subunits make contacts with one of two sites in the domain P of purple-colored gp10 subunits (1,3,6,8 with one site and 10 with the other site). The remaining 2 portal subunits (5,11) have no apparent density connecting to any gp10 subunit. The region of the portal density that associates with the gp10 subunits does not follow a strict 12-fold symmetry, whereas the gp10 subunits around the portal appear to be in a similar conformation as in the icosahedral reconstruction. Thus the symmetry mismatch at this pentameric interface is accommodated by multiple types of interactions between the structurally uniform gp10 subunits and the portal proteins.

We discovered another kind of symmetry mismatch within the portal vertex complex. The 12 copies of the adaptor constitute a ring of 6 lambda-shaped (Λ) dimers (Fig. 3c), which mediate the mismatch between the 12-fold symmetric portal and the 6-fold symmetric nozzle. The two types of symmetry of the adaptor proteins along their length may be used to accommodate the transition from one symmetry type (12-fold) to another (6-fold). On the portal side, two adjacent adaptor subunits interact with each of the 12 portal subunits (Fig. 3d), while on the other side, four contiguous adaptor subunits interact with each of the 6 nozzle subunits (Fig. 3e). In addition, two adjacent adaptor dimers are bound together through one petal of a tail fiber (Figs 2c,d and 3d). The fiber also binds to the nozzle near the valve and an adaptor subunit near the nozzle side (Figs 2c,d and 3e). This intertwined organization of the portal vertex components linked by tail fibers creates extensive interactions, which may facilitate cooperative motions among them during phage-host infection resulting in viral genome release.

Difference between full and empty particles

Cryo-EM micrographs show a small percentage of P-SSP7 particles without DNA (Fig. 1a). An asymmetric reconstruction of empty particles was also performed, but at lower resolution (24 Å) due to the limited number of particles in the data set (Fig. 2e–g). The diameter of the empty capsid was the same as that of the DNA-containing phage, whereas the portal vertex of the empty phage was different (Fig. 2, and the portal complex difference map in Supplementary Fig. 7). Empty particles lacked the “nozzle valve” and core protein densities, the distal tip of the nozzle was shaped differently, the fibers were extended horizontally rather than pointing parallel to the capsid surface, the Q-rich motifs of the portal appeared disordered and the core protein disappeared. We presume that these empty particles have completed release of their genomes and that these structural differences reflect the changes necessary to allow the DNA to exit the capsid. If true, then the changes in fiber orientation from inclined to horizontal positions may trigger co-operative structural changes in the nozzle, adaptor, portal, and core. Interestingly, signaling or structural changes from the tail fiber, which is ∼150 Å away from the Q-rich motifs, may directly influence its disordering and the disappearance of the surrounding core proteins.

Close examination of the tail fiber in full versus empty phages at equivalent resolution (Fig. 2d,g and Supplementary Fig. 7) shows that the three “petals” of the tail fiber do not undergo large movement, unlike the more distal portion of the tail fiber. However, in the full phage, the proximal end of the tail fiber (Fig. 2c) closely contacts with an adaptor subunit (yellow box in Fig. 2d), whereas in the empty phage, the density near the contact point is missing, having moved or become disordered (yellow box in Fig. 2g). In addition, the densities near the nozzle valve and the adaptor domains that are in contact with this tail fiber density also move or become disordered in the empty phage (Fig. 2d,g). These changes result in opening the “nozzle valve”, presumably allowing ejection of the dsDNA from the capsid. A similar mechanism has been indirectly inferred for phages T7[35], T4[36] and SPP1[17],[18]. Our study provides a direct evidence for this mechanism based on visualization of the valve features that are present in mature but not in empty phages.

Tomographic reconstruction of phages during cell infection

To seek additional evidence of structural changes in the portal vertex complex that may be necessary for infection *in vivo*, we used cryo-ET to examine the P-SSP7 portal vertex complex during the actual infection process. Four different phage states can be observed: free particles with and without DNA, and attached particles with and without DNA. Free particles with DNA are called free phages; attached particles with DNA are referred to as infecting particles; and empty particles are designated as post-infection phages. A slice through a representative tomogram, (Fig. 4a, Supplementary Movie 3) shows several of these states. From 12 tomograms, 29 pre-infection, 26 infecting and 8 cell-bound post-infection phages were extracted, aligned and averaged separately. The averaged density of the 26 infecting phages and the central section are shown in Fig. 4b and 4c, respectively. In contrast to the pre-infection phages, the tail fibers of the infecting phages are extended horizontally even though there was still DNA density inside the capsid. The key observation is that the change in conformation of the tail fibers precedes DNA release, and thus may be part of the triggering mechanism itself. The averaged density of the cell-bound post-infection phages also shows horizontally extended fibers. This conformation corresponds to what was seen in the single particle asymmetric reconstruction of empty phage in Fig. 2e and 2f.

Discussion

Structure of the mature P-SSP7 phage

We used single particle cryo-EM to determine the icosahedral structure of the mature P-SSP7 phage at 4.6 Å resolution (Fig. 1). This structure is among a few examples of virus particles whose Cα backbone can be traced without reference to any known crystal structure[9,37]. The topology of the P-SSP7 capsid protein bears a remarkable resemblance to HK97 and ε15 phage, whose capsid structures were previously determined at high resolution. As shown in the more detailed comparison among these phage structures (Supplementary Fig. 2), they exhibit different types of molecular interactions within and across capsomeres, which may be critical for maintaining particle stability in a mature state. Our study reiterates the now commonly observed conservation of structural motif in proteins that form a functional “nanocage” to store and safeguard viral genome material, in spite of their high sequence diversity.

Little was known about the structure of portal vertex complex until the recent advances in cryo-EM, which enabled virus structures to be solved without imposing icosahedral symmetry[30,32,35,38-40]. The reconstruction software used in this study was designed to determine at which of the 12 vertices the very low contrast and relatively small portal vertex complex resides. The sub-nanometer resolution structure of the entire P-SSP7 phage, including the portal vertex complex, gives an unambiguous view of the spatial organization of all the protein components in the portal vertex complex. Our 9 Å resolution map (Fig. 2a) is sufficient to reliably detect long α helices and large β sheets (Supplementary Fig. 4), as in previous cryo-EM maps[9,30,41]. However, the challenge remains to delineate which densities in our map correspond to which gene products. Our strategy uses a combination of proteomics, genomics and structural informatics analyses to allow us to annotate the

densities in the portal vertex complex. Because of the potential overlap of densities among neighboring proteins, it is by no means certain that the assignment of the molecular boundary of each protein is precisely correct at the current resolution. However, we are highly confident in the following conceptual conclusions drawn from our structural analyses: the conformationally heterogeneous dimer encompassing the 12-copy adaptor ring; the location of the C terminus of the portal protein with a Q-rich motif; the nozzle valve blocking the exit pathway of the DNA; a massive core protein density next to the portal pointing toward the center of the particle; the orientations of the tail fiber with respect to the portal vertex axis; a 250 Å long and 20 Å wide terminal end of dsDNA with a strand separation close to the mid point of the portal protein. Even though there have been many structural studies of phages either as a whole or in parts, most of our observed structural features of P-SSP7 have not been seen in prior studies of phage structure. Furthermore, the delineation of the molecular interface among the nozzle, adaptor, portal, tail fiber and capsid protein provides a fresh and direct glimpse at the complexity of interactions that accommodate the symmetry mismatches among these molecular components. Interestingly, by fitting the capsid backbone models into the 10 subunit densities surrounding the 12 copies of the portal protein (Fig. 3a,b), we find no apparent structural deformation of the capsid protein at our current resolution level.

Structure of the empty P-SSP7 phage

Our purified sample of P-SSP7 phages contained a small percentage of the particles that appeared to be devoid of internal DNA (Fig. 1a). We sampled those particles and obtained a 24 Å resolution map of the empty phage (Fig 2e). The low-resolution structure is due to the limited number of empty particles available in the data pool. To compare the mature and empty phage maps (Figs 2d,g; Supplementary Fig. 7) in a meaningful way, we blurred the resolution of the mature phage map (Fig. 2a) equivalent to that of the empty phage (Fig. 2e). The obvious differences in the empty phage map relative to the mature map are: the absence of DNA density; the disappearance of the nozzle valve, the change in the fiber orientation with respect to the portal vertex axis, and the disintegration of the C-terminus of the portal and of the core protein. A close examination of the molecular interfacial region among the adaptor, tail fiber and portal also shows unambiguous differences in density connectivity between the mature and empty phage structures (Fig. 2d,g and Supplementary Fig. 7).

Cryo-ET Structure of P-SSP7 attached to *Prochlorococcus*

Cryo-ET is an emerging method for reconstructing the 3-D structure of one sample at a time[42,43]. Cryo-ET is a low-resolution technique because of the radiation damage to specimens resulting from multiple electron exposures, but it is extremely powerful for revealing structures that may vary from one cell to another and therefore cannot be averaged as in a single particle reconstruction. In this study, we focused on the extraction of the structures of phage particles attached to the host cell surface. Using post-tomographic classification, aligning and averaging of the sub-volumes of the computationally extracted phage particles attached to the cell, we were able to find a subpopulation of phage particles in which the DNA was still present, but the tail fiber was oriented similarly to that of the empty phage (Fig. 4b,c and Fig. 2e,f). This match supports the hypothesis that the phage tail fiber orientation changes while attached to the host surface *in vivo* before DNA release. Our

study represents the first example of applying cryo-ET to correlate the observed high-resolution structural features of a virus to its structure in the context of a host cell.

Plausible model of viral genome release

Based on both single particle reconstructions of individual phages and tomographic reconstructions of phages actively infecting the host cell, we propose a mechanism for DNA release from the phage as follows. First, the most distal segments of the tail fibers explore the host cell surface in search of a binding site to initiate the infection. As in phage T7[23,44], the phage orients itself with its portal vertex complex pointing perpendicular to the cell surface so that the tail nozzle is in contact with the cell surface and the proximal segments of the fibers extend horizontally (Fig. 4d). This tail fiber orientation change in turn affects the interactions among the tail fiber, adaptor and the portal causing the Q-rich motifs of the portal protein to loosen, thereby triggering the internal core proteins to disassemble. During this process, the DNA structure may also be changed and thus could contribute to the disassembly of the Q-motifs of the portal protein and the core proteins. Not the least among the structural change is found in the opening of the "nozzle valve" (Fig. 2b–d and 2f,g). The cumulative conformational changes in the portal vertex complex should then finally allow the phage DNA to eject freely.

In all, this study demonstrates the power of using cryo-EM and cryo-ET synergistically both *in vitro* and *in vivo*, particularly for non-icosahedrally arranged protein components at a broad range of resolutions. The structures provide a number of structural features of the P-SSP7 phage in different functional states, which have not been seen in previous studies of other dsDNA viruses. Also, our structural interpretation sheds light on the biology of a T7-like phage and the long-standing mystery of DNA delivery from phage to host[45,46]. Given that this phage type is a prominent member of the global oceanic phage community, such findings not only impact our understanding of this ecologically important phage-host system, but also refine our view of a biological process using a complex protein machinery to transfer the viral genome to an infected cell.

Methods

Methods and any associated references are available in the online version of the paper at http://www.nature.com/nsmb/.

Supplementary Material

Refer to Web version on PubMed Central for supplementary material.

Acknowledgments

This research was supported in parts by grants from NIH (P41RR002250, R01GM079429 to W.C.), NSF (IIS-0705644 to W.C. and M.L.B.), the Robert Welch Foundation (Q1242 to W.C.), NSF, DOE and the Gordon and Betty Moore Foundation (to S.W.C.). We thank Maureen Coleman, Sebastien Rodrigue, Rex Malmstrom, Jake Waldbauer and Suzanne Kern for assistance in the infection experiments; Juan Chang, Qinglu Zeng, Simon Labrie, and Frazer Rixon for discussions; Juan Chang, Kurt Welgehausen and Ryan Rochat for editorial assistance in preparation of the manuscript.

References

1. Sullivan MB, Coleman ML, Weigele P, Rohwer F, Chisholm SW. Three Prochlorococcus cyanophage genomes: signature features and ecological interpretations. PLoS Biol. 2005; 3:e144. [PubMed: 15828858]
2. Moore LR, Rocap G, Chisholm SW. Physiology and molecular phylogeny of coexisting Prochlorococcus ecotypes. Nature. 1998; 393:464–7. [PubMed: 9624000]
3. Liu H, Nolla HA, Campbell L. Prochlorococcus growth rate and contribution to primary production in the equatorial and subtropical North Pacific Ocean. Aquatic Microbial Ecology. 1997; 12:39–47.
4. Angly FE, et al. The marine viromes of four oceanic regions. PLoS Biol. 2006; 4:e368. [PubMed: 17090214]
5. Lindell D, et al. Genome-wide expression dynamics of a marine virus and host reveal features of co-evolution. Nature. 2007; 449:83–6. [PubMed: 17805294]
6. Lindell D, Jaffe JD, Johnson ZI, Church GM, Chisholm SW. Photosynthesis genes in marine viruses yield proteins during host infection. Nature. 2005; 438:86–9. [PubMed: 16222247]
7. Liu X, Jiang W, Jakana J, Chiu W. Averaging tens to hundreds of icosahedral particle images to resolve protein secondary structure elements using a Multi-Path Simulated Annealing optimization algorithm. J Struct Biol. 2007; 160:11–27. [PubMed: 17698370]
8. Ludtke SJ, Baldwin PR, Chiu W. EMAN: semiautomated software for high-resolution single-particle reconstructions. J Struct Biol. 1999; 128:82–97. [PubMed: 10600563]
9. Jiang W, et al. Backbone structure of the infectious epsilon15 virus capsid revealed by electron cryomicroscopy. Nature. 2008; 451:1130–4. [PubMed: 18305544]
10. Wikoff WR, et al. Topologically linked protein rings in the bacteriophage HK97 capsid. Science. 2000; 289:2129–33. [PubMed: 11000116]
11. Jiang W, et al. Coat protein fold and maturation transition of bacteriophage P22 seen at subnanometer resolutions. Nat Struct Biol. 2003; 10:131–5. [PubMed: 12536205]
12. Fokine A, et al. Structural and functional similarities between the capsid proteins of bacteriophages T4 and HK97 point to a common ancestry. Proc Natl Acad Sci U S A. 2005; 102:7163–8. [PubMed: 15878991]
13. Morais MC, et al. Conservation of the capsid structure in tailed dsDNA bacteriophages: the pseudoatomic structure of phi29. Mol Cell. 2005; 18:149–59. [PubMed: 15837419]
14. Baker ML, et al. Architecture of the herpes simplex virus major capsid protein derived from structural bioinformatics. J Mol Biol. 2003; 331:447–56. [PubMed: 12888351]
15. Purohit PK, et al. Forces during bacteriophage DNA packaging and ejection. Biophys J. 2005; 88:851–66. [PubMed: 15556983]
16. Aksyuk AA, et al. The tail sheath structure of bacteriophage T4: a molecular machine for infecting bacteria. EMBO J. 2009; 28:821–9. [PubMed: 19229296]
17. Orlova EV, et al. Structure of a viral DNA gatekeeper at 10 A resolution by cryo-electron microscopy. EMBO J. 2003; 22:1255–62. [PubMed: 12628918]
18. Lhuillier S, et al. Structure of bacteriophage SPP1 head-to-tail connection reveals mechanism for viral DNA gating. Proc Natl Acad Sci U S A. 2009; 106:8507–12. [PubMed: 19433794]
19. Leiman PG, Chipman PR, Kostyuchenko VA, Mesyanzhinov VV, Rossmann MG. Three-dimensional rearrangement of proteins in the tail of bacteriophage T4 on infection of its host. Cell. 2004; 118:419–29. [PubMed: 15315755]
20. Plisson C, et al. Structure of bacteriophage SPP1 tail reveals trigger for DNA ejection. EMBO J. 2007; 26:3720–8. [PubMed: 17611601]
21. Cong Y, et al. Structural mechanism of SDS-induced enzyme activity of scorpion hemocyanin revealed by electron cryomicroscopy. Structure. 2009; 17:749–58. [PubMed: 19446530]
22. Henderson R, Moffat JK. The difference Fourier technique in protein crystallography: errors and their treatment. Acta Crystallogr B. 1971; 27:7.
23. Kemp P, Garcia LR, Molineux IJ. Changes in bacteriophage T7 virion structure at the initiation of infection. Virology. 2005; 340:307–17. [PubMed: 16054667]

24. Baker ML, Ju T, Chiu W. Identification of secondary structure elements in intermediate-resolution density maps. Structure. 2007; 15:7–19. [PubMed: 17223528]
25. Simpson AA, et al. Structure determination of the head-tail connector of bacteriophage phi29. Acta Crystallogr D. 2001; 57:1260–9. [PubMed: 11526317]
26. Lebedev AA, et al. Structural framework for DNA translocation via the viral portal protein. EMBO J. 2007; 26:1984–94. [PubMed: 17363899]
27. McGuffin LJ, Bryson K, Jones DT. The PSIPRED protein structure prediction server. Bioinformatics. 2000; 16:404–5. [PubMed: 10869041]
28. Cole C, Barber JD, Barton GJ. The Jpred 3 secondary structure prediction server. Nucleic Acids Res. 2008; 36:W197–201. [PubMed: 18463136]
29. Guo L, Han A, Bates DL, Cao J, Chen L. Crystal structure of a conserved N-terminal domain of histone deacetylase 4 reveals functional insights into glutamine-rich domains. Proc Natl Acad Sci U S A. 2007; 104:4297–302. [PubMed: 17360518]
30. Jiang W, et al. Structure of epsilon15 bacteriophage reveals genome organization and DNA packaging/injection apparatus. Nature. 2006; 439:612–6. [PubMed: 16452981]
31. Randall GL, Zechiedrich L, Pettitt BM. In the absence of writhe, DNA relieves torsional stress with localized, sequence-dependent structural failure to preserve B-form. Nucleic Acids Res. 2009
32. Tang J, et al. DNA poised for release in bacteriophage phi29. Structure. 2008; 16:935–43. [PubMed: 18547525]
33. Hendrix RW. Symmetry mismatch and DNA packaging in large bacteriophages. Proc Natl Acad Sci U S A. 1978; 75:4779–83. [PubMed: 283391]
34. Simpson AA, et al. Structure of the bacteriophage phi29 DNA packaging motor. Nature. 2000; 408:745–50. [PubMed: 11130079]
35. Agirrezabala X, et al. Maturation of phage T7 involves structural modification of both shell and inner core components. EMBO J. 2005; 24:3820–9. [PubMed: 16211007]
36. Kostyuchenko VA, et al. The tail structure of bacteriophage T4 and its mechanism of contraction. Nat Struct Mol Biol. 2005; 12:810–3. [PubMed: 16116440]
37. Yu X, Jin L, Zhou ZH. 3.88 A structure of cytoplasmic polyhedrosis virus by cryo-electron microscopy. Nature. 2008; 453:415–9. [PubMed: 18449192]
38. Lander GC, et al. The structure of an infectious P22 virion shows the signal for headful DNA packaging. Science. 2006; 312:1791–5. [PubMed: 16709746]
39. Leiman PG, et al. The structures of bacteriophages K1E and K1-5 explain processive degradation of polysaccharide capsules and evolution of new host specificities. J Mol Biol. 2007; 371:836–49. [PubMed: 17585937]
40. Xiang Y, et al. Structural changes of bacteriophage phi29 upon DNA packaging and release. EMBO J. 2006; 25:5229–39. [PubMed: 17053784]
41. Serysheva II, et al. Subnanometer-resolution electron cryomicroscopy-based domain models for the cytoplasmic region of skeletal muscle RyR channel. Proc Natl Acad Sci U S A. 2008; 105:9610–5. [PubMed: 18621707]
42. Baker, ML.; Marsh, MP.; Chiu, W. Cryo-EM of molecular nanomachines and cells. In: Vogel, V., editor. Nanotechnology. Vol. 5. Wiley VCH, Verlag GmbH & Co. KGaA; Weinheim: 2009. p. 91-111.
43. Lucic V, Forster F, Baumeister W. Structural studies by electron tomography: from cells to molecules. Annu Rev Biochem. 2005; 74:833–65. [PubMed: 15952904]
44. Steven AC, et al. Molecular substructure of a viral receptor-recognition protein. The gp17 tail-fiber of bacteriophage T7. J Mol Biol. 1988; 200:351–65. [PubMed: 3259634]
45. Molineux IJ. No syringes please, ejection of phage T7 DNA from the virion is enzyme driven. Mol Microbiol. 2001; 40:1–8. [PubMed: 11298271]
46. Molineux, IJ.; Calendar, R.; Abedon, ST. The Bacteriophages. Vol. 17. Oxford University Press; USA: 2006. The T7 group.
47. Kivioja T, Ravantti J, Verkhovsky A, Ukkonen E, Bamford D. Local average intensity-based method for identifying spherical particles in electron micrographs. J Struct Biol. 2000; 131:126–34. [PubMed: 11042083]

48. Crowther RA, DeRosier DJ, Klug A. The reconstruction of a three-dimensional structure from projections and its application to electron microscopy. Proc Roy Soc Lond A. 1970; 317:319–340.

49. Chang J, Weigele P, King J, Chiu W, Jiang W. Cryo-EM asymmetric reconstruction of bacteriophage P22 reveals organization of its DNA packaging and infecting machinery. Structure. 2006; 14:1073–82. [PubMed: 16730179]

50. Pettersen EF, et al. UCSF Chimera--a visualization system for exploratory research and analysis. J Comput Chem. 2004; 25:1605–12. [PubMed: 15264254]

51. Ludtke SJ, et al. De Novo backbone trace of GroEL from single particle electron cryomicroscopy. Structure. 2008; 16:441–8. [PubMed: 18334219]

52. Mastronarde DN. Automated electron microscope tomography using robust prediction of specimen movements. J Struct Biol. 2005; 152:36–51. [PubMed: 16182563]

53. Kremer JR, Mastronarde DN, McIntosh JR. Computer visualization of three-dimensional image data using IMOD. J Struct Biol. 1996; 116:71–6. [PubMed: 8742726]

54. Schmid MF, Booth CR. Methods for aligning and for averaging 3D volumes with missing data. J Struct Biol. 2008; 161:243–8. [PubMed: 18299206]

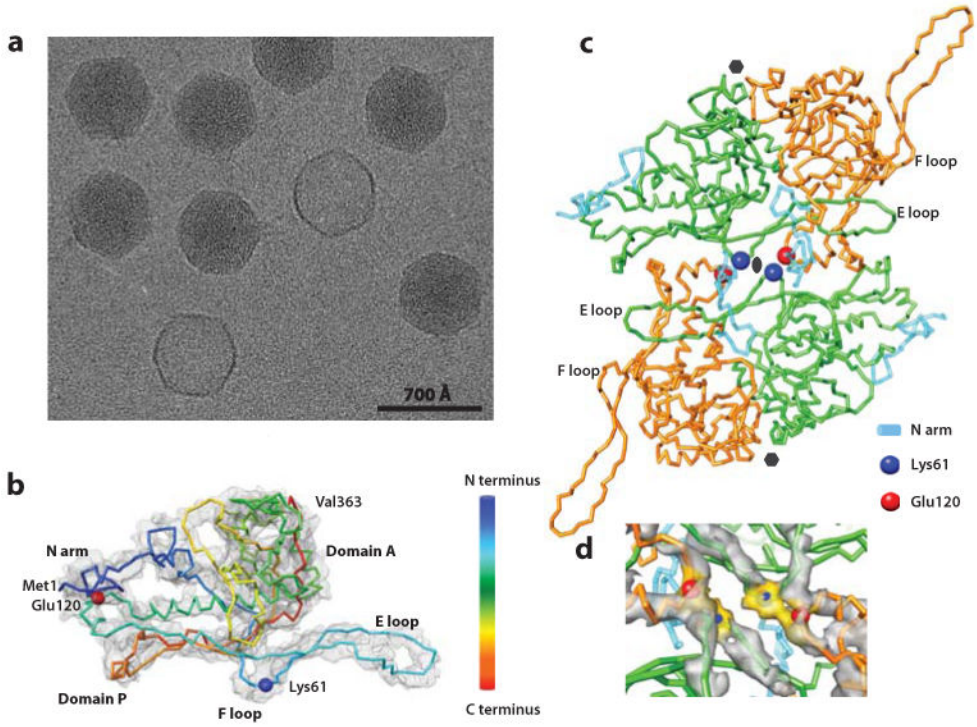

Figure 1. Image and reconstruction of P-SSP7 at 4.6 Å resolution

(a) 300kV image of P-SSP7 embedded in vitreous ice. **(b)** Segmented density of the shell protein subunit (gp10) and its Cα model from the 4.6 Å icosahedral reconstruction. **(c)** Subunit interactions within and across capsomeres. Four subunits are shown; the upper two belong to one pseudo-6 fold capsomere, the bottom two belong to another capsomere. The view is from the outside of the capsid looking almost down the 2-fold symmetry axis. **(d)** A zoomed-in view, but viewed from inside the capsid, with the corresponding density around the F loop and domain P. The densities (annotated in yellow) near the 2-fold axis indicate interactions between Lys61 (in blue) and Glu120 (in red) from two capsomeres.

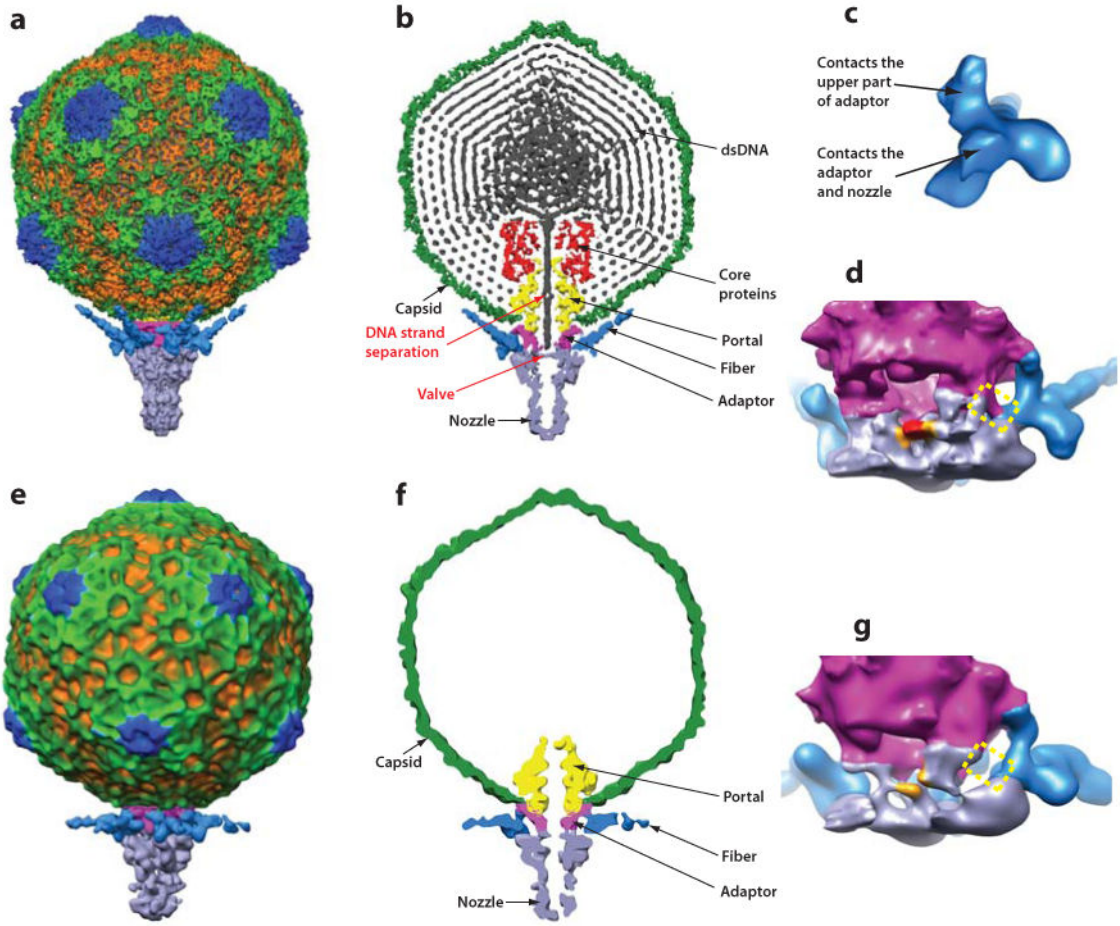

Figure 2. Asymmetric reconstructions of P-SSP7

(a) 9.2 Å resolution map of the full phage. **(b)** Central slice of the full phage. **(c)** Fiber trimer viewed from its proximal end. **(d)** A cutaway zoomed-in view of the adaptor, nozzle and tail fibers. In (c) and (d), the full phage map was low-pass filtered to the same resolution as the empty phage map to facilitate comparison between the structures. **(e)** 24 Å resolution asymmetric reconstruction of the empty phages. **(f)** Central slice of the empty phage. **(g)** Cutaway view for the empty phage equivalent to the view in (d). All phage protein components are annotated and colored differently. Two special features (valve density and DNA strand separation) are observed in the slice from the full phage (b). There are substantial conformational changes in the nozzle, tail fibers, portal and core proteins between the full and empty particles. The yellow dashed box in (d) shows that a fiber interacts with both nozzle and adaptor in full phage, but the links between fiber and adaptor are broken in empty phage (g). The full phage has strong density at and around the valve (colored in orange and red), but the density of empty phage in the corresponding location is markedly reduced and there is no density at the valve.

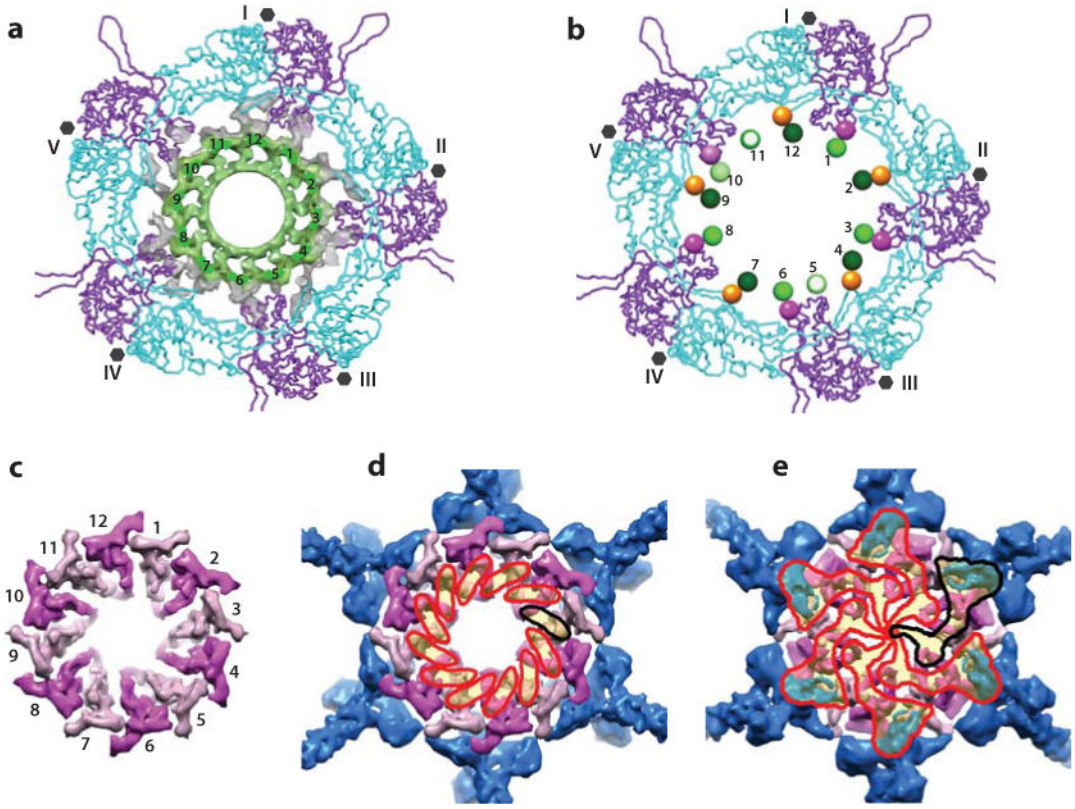

Figure 3. Symmetry mismatch at the portal vertex

(a) Interface between 12 copies of portal (greenish) and 10 copies of gp10 models (purple and cyan). The purple and cyan molecules represent two subunits from each of the 5 surrounding hexons. The gray density segmented from the asymmetric reconstruction is the interfacial density between capsid and portal. **(b)** Schematic diagram to illustrate the 4 apparent types of interactions in our density map: F loop interaction (2, 4, 7, 9, 12), hook of domain P interaction (1, 3, 6, 8), N terminus of long helix interaction (10) and no interaction (5, 11). **(c)** 12 copies of adaptor proteins in alternating conformations. **(d)** Interface between the portal (red and black footprints – black indicates one subunit) and the adaptor. One subunit of the portal interacts with two neighboring adaptor subunits. **(e)** Interface between the nozzle (red and black footprints, black for 1 subunit) and the adaptor. One nozzle subunit interacts with 4 contiguous adaptor subunits and also interacts with a tail fiber. The nozzle footprint outlines coverage around the center of the nozzle and indicates the presence of the "valve". Figure 3a, 3b and 3e are viewed from the outside along the portal vertex complex axis, while Figure 3c and 3d are viewed from the inside of the capsid.

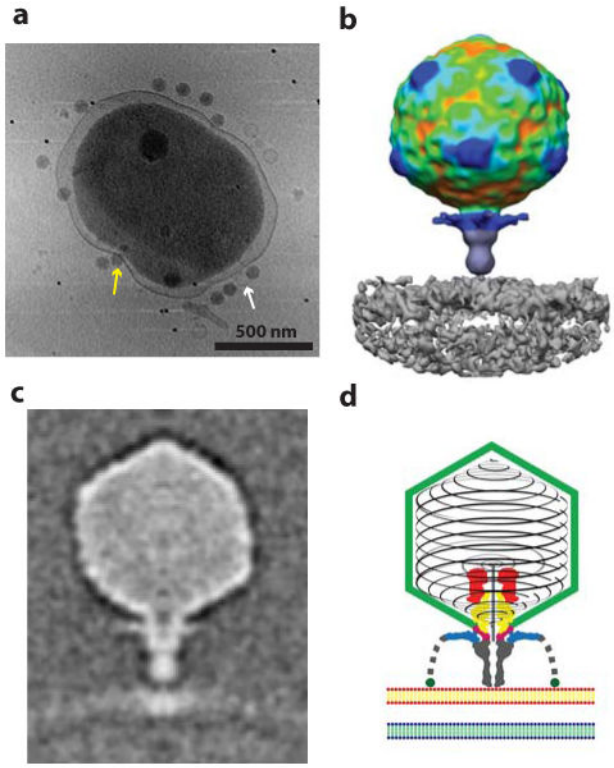

Figure 4. Cryo-ET of P-SSP7 infecting MED-4 cell

(a) Slice of a tomogram showing three states of P-SSP7 in its native environment: infecting phages (all dark particles with one annotated by a yellow arrow); post-infection (empty) phages still attached to the cell (white arrow); and unattached phages. The attachment of the phages to the host cell can only be ascertained from the visualization of the 3-D tomogram, but not in a 2-D slice as exemplified here. **(b)** An average of 26 infecting phage subtomograms with the portal vertex oriented normal to the cell surface. The phage tail fibers are extended horizontally. **(c)** Central slice of the averaged subtomograms of infecting phages. **(d)** Schematic cartoon of P-SSP7 phage infecting the host cell (the cell membranes are represented by the double layer at the bottom).